Atmos. Chem. Phys., 10, 8881–8897, 2010
www.atmos-chem-phys.net/10/8881/2010/
doi:10.5194/acp-10-8881-2010

Atmospheric Chemistry and Physics

CO_2 and its correlation with CO at a rural site near Beijing: implications for combustion efficiency in China

Y. Wang[1], J. W. Munger[2], S. Xu[1], M. B. McElroy[2], J. Hao[1], C. P. Nielsen[3], and H. Ma[1]

[1]Department of Environmental Science and Engineering and State Key Joint Laboratory of Environment Simulation and Pollution, Tsinghua University, Beijing, China
[2]Department of Earth and Planetary Sciences and School of Engineering and Applied Sciences, Harvard University, Cambridge, Massachusetts, USA
[3]Harvard China Project and School of Engineering and Applied Sciences, Harvard University, Cambridge, Massachusetts, USA

Received: 20 April 2010 – Published in Atmos. Chem. Phys. Discuss.: 17 May 2010
Revised: 1 September 2010 – Accepted: 6 September 2010 – Published: 21 September 2010

Abstract. Although China has surpassed the United States as the world's largest carbon dioxide emitter, in situ measurements of atmospheric CO_2 have been sparse in China. This paper analyzes hourly CO_2 and its correlation with CO at Miyun, a rural site near Beijing, over a period of 51 months (Dec 2004 through Feb 2009). The CO_2-CO correlation analysis evaluated separately for each hour of the day provides useful information with statistical significance even in the growing season. We found that the intercept, representing the initial condition imposed by global distribution of CO_2 with influence of photosynthesis and respiration, exhibits diurnal cycles differing by season. The background CO_2 ($CO_{2,b}$) derived from Miyun observations is comparable to CO_2 observed at a Mongolian background station to the northwest. Annual growth of overall mean CO_2 at Miyun is estimated at 2.7 ppm yr^{-1} while that of $CO_{2,b}$ is only 1.7 ppm yr^{-1} similar to the mean growth rate at northern mid-latitude background stations. This suggests a relatively faster increase in the regional CO_2 sources in China than the global average, consistent with bottom-up studies of CO_2 emissions. For air masses with trajectories through the northern China boundary layer, mean winter CO_2/CO correlation slopes (dCO_2/dCO) increased by 2.8 ± 0.9 ppmv/ppmv or 11% from 2005–2006 to 2007–2008, with CO_2 increasing by 1.8 ppmv. The increase in dCO_2/dCO indicates improvement in overall combustion efficiency over northern China after winter 2007, attributed to pollution reduction measures associated with the 2008 Beijing Olympics. The observed CO_2/CO ratio at Miyun is 25% higher than the bottom-up CO_2/CO emission ratio, suggesting a contribution of respired CO_2 from urban residents as well as agricultural soils and livestock in the observations and uncertainty in the emission estimates.

Correspondence to: Y. Wang
(yxw@tsinghua.edu.cn)

1 Introduction

Carbon dioxide (CO_2) is an important greenhouse gas. Enhanced CO_2 level in the atmosphere and its relationship with global climate change have not only drawn increasing attention from the scientific community but also presented great political and economic challenges to the entire world. A number of factors influence atmospheric CO_2 mixing ratios. Long-term increase in CO_2 following the Industrial Revolution is attributed to emissions from human activity, especially fossil fuel combustion. A fraction of anthropogenic emissions is absorbed by ocean and terrestrial biosphere. Together ocean and terrestrial biosphere uptake take up about 60% of CO_2 emissions. The fraction of emitted CO_2 that remains in the atmosphere has large interannual variability, attributed in part to global climate anomalies such as ENSO (Keeling et al., 1976). The terrestrial biosphere regulates the amplitude and phase of CO_2 seasonal cycles (Fung et al., 1987; Keeling et al., 1989; Taguchi, 1996). Net accumulation of carbon by forests in the northern hemisphere is thought to be an important mechanism in maintaining the current hemispheric gradient in CO_2 (Tans et al., 1990; Wofsy et al., 1993; Fan et al., 1998). Global network of atmospheric CO_2 observations, including the National Oceanic

Published by Copernicus Publications on behalf of the European Geosciences Union.

and Atmospheric Administration (NOAA) Earth System Research Laboratory (ESRL) background stations, has contributed to the progress in our understanding of the global carbon budget.

The most recent energy use and emission inventories indicate that China surpassed the United States as the world's largest carbon emitter in 2006 (Gregg et al., 2008). China's recent economic growth has been largely fueled by fossil energy, particularly coal. In 2006, China's energy-related emissions of CO_2 reached approximately 1.6 Pg C (Levine and Aden, 2008). Most estimates of China's energy-related carbon emissions are derived from official energy statistics, which are subject to large uncertainties. Based on inventories of biomass and soil carbon, ecosystem models, and atmospheric inversions, it is estimated that the biosphere in China removed roughly 28–37% of Chinese fossil fuel CO_2 emissions during the 1980s and 1990s (Piao et al., 2009). The overall CO_2 budget of China has large uncertainties. Observations of CO_2 variations in the atmosphere, reflecting the combined effect of all sources and sinks, would provide additional constraints to reduce uncertainty in bottom-up estimates of natural and anthropogenic components of the Chinese carbon budget.

Significant improvement in current understanding of the related processes and evaluation of bottom-up emission inventories of CO_2 will require an extensive network of CO_2 observations in China. Among all NOAA/ESRL background stations distributed globally, there are two adjacent sites upwind and downwind of China, Ulaan Uul (UUM) in Mongolia and Tae-ahn Peninsula (TAP) in South Korea respectively (Fig. 1a). The Chinese Academy of Meteorological Sciences operates Waliguan Baseline Observatory (WLG) at Mount Waliguan (WLG) on the Qinghai-Tibet Plateau (Fig. 1a) in mainland China which has provided background atmospheric CO_2 data since 1991 (Zhou et al., 2005, 2003). CO_2 at WLG is dominated mostly by the exchange between the atmosphere and terrestrial biosphere (Zhou et al., 2006). Similar to other background stations, the inter-annual variability of CO_2 at WLG – after the removal of the trend – is influenced by the long-range transport of pollution. However, because of its high elevation the observations at WLG are weakly influenced by local and regional CO_2 sources and sinks, thus providing limited information about anthropogenic CO_2 emissions in China, but offering a good representation of global background CO_2 signal that influences surface observations throughout China by vertical mixing. There are a few background CO_2 sites located downwind of China. Continuous monitoring of CO_2 at those sites provided some implications of carbon emissions and uptakes from China. Cho et al. (2007) studied the continuous CO_2 measurements at Anmyeondo, South Korea from 1999 to 2006, and attributed the 2.6 ppmv/yr growth rate of atmospheric CO_2 to the recent industrialization and urbanization of Korea and China. Jin et al. (2008) reported a continuous 1-year atmospheric CO_2 measurement at Gosan, Seoul,

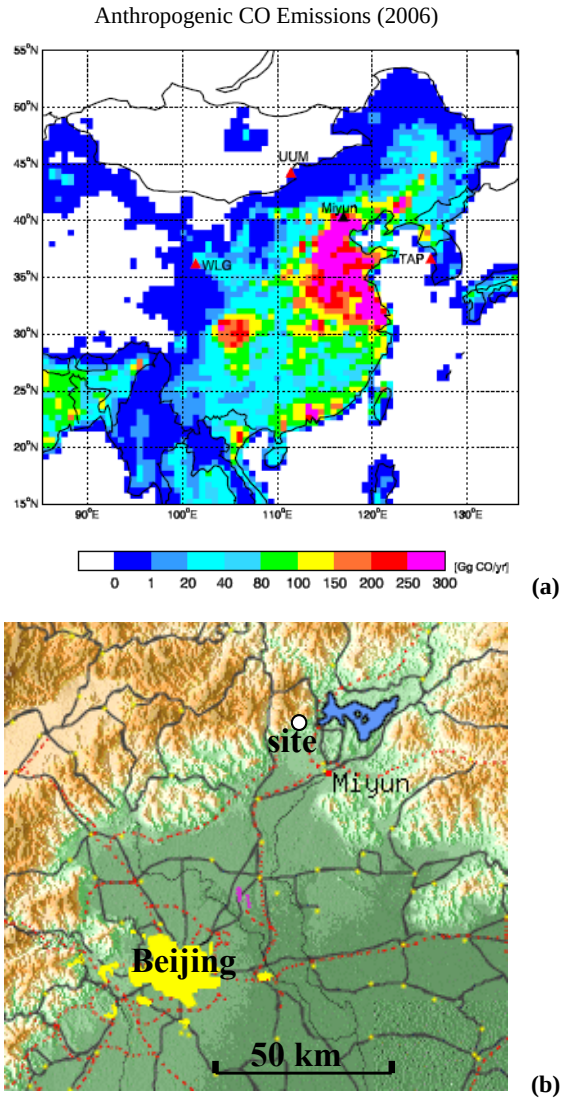

Fig. 1. **(a)** Locations of the Miyun site (filled black triangle) and several background sites in and around China (WLG, UUM, TAP) (filled red triangles). The color shading indicates anthropogenic CO emissions for 2006 (Zhang et al., 2009). **(b)** A regional map shows the location of the site (white circle) relative to Beijing urban area and other population centers(yellow), major roads (red), airport (magenta), and terrain. The color shading indicates elevation from low (green – near sea level) to high (darkest brown corresponding to 1400 m). Miyun city is indicated by the red dot. Reproduced from Wang et al. (2008)

and Yanbian stations during 2004–2005, and using a chemical transport model identified the potential source regions as the northeastern and eastern parts of China. Zhang et al. (2008) analyzed the atmospheric CO_2 mixing ratio obtained via a regular flask air sampling program onboard a ferry in the southernmost part of Japan from 1993 to 2006 and found some mixing ratios with large deviation from global mean CO_2, which could have resulted from terrestrial biotic activity in China. The gradient in CO_2 between Mongolia and

Korea may shed some light on the net source or sink of CO_2 over China. The Miyun observatory outside Beijing was established to address the paucity of continuous high quality trace gas measurements within China. Here we examine the potential for the resulting data to better constrain estimates of local to regional carbon budgets.

CO is a product of inefficient combustion that has often been used as a tracer of CO_2 from combustion (Bakwin et al., 1997; Potosnak et al., 1999; Turnbull et al., 2006). The emission ratio of CO_2 to CO varies with the efficiency of combustion (Andreae and Merlet, 2001). Observed CO_2-CO correlation slopes thus provide useful constraints for identifying source types. For example, in modern power plants burning fossil fuels conversion of fuel carbon to CO_2 is nearly quantitative, whereas in biomass combustion with low fuel to air ratios 10% or more of carbon remains as CO. Consequently, the CO_2/CO ratio observed in power plant plumes, derived conventionally from the CO_2-CO correlation slope, should be an order of magnitude greater than the ratio in biomass burning plumes. The emission ratio of CO_2 to CO from vehicles varies significantly depending on emission control technologies adopted and vehicle maintenance. Vehicle CO_2 to CO emission ratios in the US derived from tunnel measurements increased from about 10 ppmv/ppmv for pre-1975 vehicles to 50 ppmv/ppmv for vehicles in early 1990s (Bishop et al., 1996), with further increases measured for vehicles in late 1990s and early 2000s (Bishop and Stedman, 2008). Higher CO_2-CO ratios are expected from vehicles meeting the Euro IV standard that will be mandated in China in 2010. Observations during the TRACE-P aircraft campaign over the Northwest Pacific in spring 2001 of air masses influenced by northeastern China yielded a slope of 10–20 ppmv/ppmv, which is significantly lower than the slope of 80 ppmv/ppmv sampled in outflow from Japan (Suntharalingam et al., 2004). Measurements at an urban site in Beijing, after excluding background air masses, suggested a CO_2/CO ratio of 23 ppmv/ppmv in winter compared with that of 33 ppmv/ppmv in fall (Han et al., 2009). Han et al. (2009) attributed the lower ratio in winter to low efficiency domestic heating, while the higher ratio in fall would also be consistent with stronger input from respiration when it is warmer. The CO_2/CO correlation slope thus provides a characteristic signature of the source region's overall combustion efficiency, corresponding well to its mixture and distribution of energy sources.

CO_2 and CO have been measured continuously at Miyun, a rural site 100 km northeast of Beijing since December 2004. This paper presents hourly averaged data for a period of 51 months (Dec 2004 through Feb 2009). The CO_2 record at Miyun will provide valuable data for future modeling analysis of Chinese carbon sources and sinks. Hourly observations of CO_2 and its correlation with CO at Miyun are expected to provide more constraints on the local to regional influences of fossil fuel and biomass combustion and biospheric uptake and release on the abundance of CO_2 over China which cannot be obtained from background stations such as WLG alone.

China's 11th Five-Year Plan (FYP) set a target of reducing China's energy intensity (energy consumption per unit of GDP) by 20% from 2005 to 2010 (NDRC, 2006). The atmospheric CO_2 to CO ratio measured at the Miyun site will provide an additional independent constraint to the question whether there has been improvement in combustion efficiency in China during the study period, an indirect measure of the effectiveness of the 11th FYP. However, we note the distinction between combustion efficiency, which can be detected from CO_2/CO ratio, and energy intensity, which cannot be inferred from our data. In addition to this national policy incentive, the pollution reduction measures implemented on the local and regional scale to improve air quality during the 2008 Beijing Olympics are expected to contribute to changes in CO and the CO_2/CO ratio.

We begin by introducing the site and instrumentation (Sect. 2). In Sect. 3, we examine the temporal variations of CO_2 on different time scales, focusing on the different characteristics of CO_2 between rural and background sites. The CO_2 to CO correlation analysis provides a convenient method to separate contributions from different sources of CO_2. The year-to-year changes in CO_2/CO ratio at Miyun outside the growing season are discussed in Sect. 4. Section 5 explains the effect of the Olympics on the CO_2-CO relationship at Miyun. Concluding remarks are given in Sect. 6.

2 Site and instrumentation

The Miyun site (40°29′ N, 116°46.45′ E) is located at an elevation of about 152 m in Miyun County (population of about 420 000), one of the two rural counties governed by the Beijing municipality. The site is about 100 km northeast of the Beijing urban center. Beijing has a population of over 16 million and a vehicle fleet of more than 4 million at the end of 2009. Major pollution sources in Beijing are vehicle emissions, power plants, industry, residential boilers, and construction activities in the case of particulate emissions. A map of the Beijing-Miyun region is shown in Fig. 1b. There are no large point sources of pollution between the Beijing urban center and Miyun, nor close to the site in other directions. As the prevailing winds include both northwesterly and southwesterly flows under the influence of frontal passage and monsoonal patterns, the site location site was selected to capture the contrast between clean continental air and the Beijing urban plume. The surroundings about 20 km to the south of the station are dominated by agriculture and small villages. The mostly undeveloped foothills of Yansan Mountains rise to the north. The main land use types of Miyun County are forest land and grassland, which together cover more than 50% of the total area of the County (Dang et al., 2003; Zhang et al., 2007). The major vegetation types

are warm-temperate deciduous broad-leaved forest and temperate coniferous forest.

Measurements began in November 2004 and include continuous observations of CO, CO_2, and basic meteorological data (temperature, relative humidity, wind speed and direction) as well as other pollutants (O_3, NO, NO_y, SO_2). The present study focuses on hourly mean measurements of CO_2 and CO over the course of more than four years (Dec 2004 through Feb 2009). Details of the infra-red absorbance based CO instrument and calibration procedure are presented by Wang et al. (2008) and not repeated here.

The CO_2 mixing ratio is measured by the differential non-dispersive infrared (NDIR) method (LI-COR Biosciences Li-7000), shown schematically in Fig. 2. The measurement system incorporates extensive automatic calibration and active control of pressure and flow to assure reliable measurements that are compatible with global measurement standards. Sample air is drawn first into the inlet 6m above the ground and passed through a 2 °C cold trap and a Nafion dryer to reduce water vapor to a low and constant mixing ratio. The reference cell is purged with compressed air with ~375 ppmv CO_2. Active mass flow and pressure controllers installed upstream and downstream of the instrument, respectively, maintain a constant cell pressure in the analyzer. Instrument zero is determined every 2 h by passing the reference gas into both the reference and sample cells. Data are recorded as raw absorptances and converted to CO_2 mixing ratios relative to dry air using a second order polynomial fit to calibration data obtained every 6 hours by introducing CO_2 standards of high, middle and low mixing ratio that bracket the range of expected ambient mixing ratios into the sample cell. Every 7 days, the instrument accuracy is checked by introducing a separate CO_2 standard into the sample cell, and comparing the calculated mixing ratio with the known mixing ratio. The three working and surveillance standards were obtained from Scott-Marrin Inc. and calibrated to 0.1 ppm accuracy against a suite of NOAA primary standards maintained as part of a dedicated calibration system in our laboratory at Harvard that supports several other ground-based measurement sites and airborne instruments (Daube et al., 2002). Measurement of the surveillance standard is especially intended to detect long-term drifts and shifts associated with periodic replacement of the working standards. Compared with the expected mixing ratio of 382.12 ppmv (measured before shipment to the site in 2004) for the archive standard, the mean of 177 validated points over the whole study period is 382.42 ± 0.70 ppmv. Although the expected mixing ratio is not within the 95% confidence interval of the validated points (382.31−382.52 ppmv), there was no evidence of drift or calibration shifts; the slope of a linear regression of the mixing ratio over time is not significantly different from zero at 95% significance level. Because the archive standard is still in service, a post-use recalibration is not available at this time to determine if its true mixing ratio has changed since delivery to the site. The analytical precision of the CO_2 measurements derived from 1-minute standard deviations of the calibration signals is 0.08 ppm (2-σ.

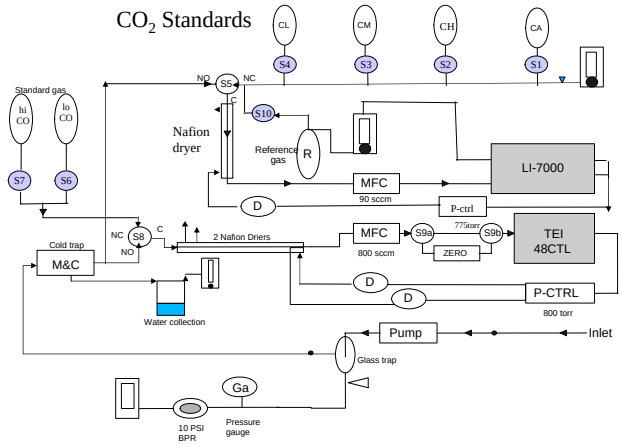

Fig. 2. Schematic of the CO_2 measurement set-up at Miyun. Sample and calibration flows are denoted by solid lines with arrowheads to indicate direction. Computer-controlled solenoid valves are indicated by shaded circles and identified as S1-10. The normally-open and normally-closed and common ports are identified by NO, NC and C. Mass-flow controllers are indicated by boxes labeled MFC, with the nominal flow rate given beneath. Likewise Pressure controllers (P-ctrl) list the nominal pressure below. Drierite traps to remove residual water in the instrument exhaust flow prior to the Nafion driers are indicated by ellipses identified with a D. Manually controlled needle valves with integrated rotometers regulate the venting of standard, to ensure rapid flushing between CO_2 calibration, and flow of reference gas. Upstream sample pressure is controlled by a back-pressure regulator (BPR) set to 10 psi; a rotometer is installed to confirm that pump output is generating an excess flow.

3 Results

3.1 General statistics of CO_2

3.1.1 Diel variations

Diel patterns of CO_2 averaged by months are shown in Fig. 3. The diel pattern is standardized by subtracting 24-hr mean CO_2 from hourly CO_2 (Murayama et al., 2004). The day/night shift between photosynthesis and respiration, boundary layer dynamics, and pollution transport all contribute to observed diel cycles in CO_2 mixing ratio, with the magnitude dependent on sampling height above the surface (Bakwin et al., 1998). Pronounced diel cycles of CO_2 can be found in summertime, with peaks at night and troughs in the afternoon, driven mostly by nighttime respiration and daytime CO_2 drawdown by photosynthesis in the surrounding region. The diel cycles are relatively flat in winter indicating that biological fluxes are more constant throughout the day.

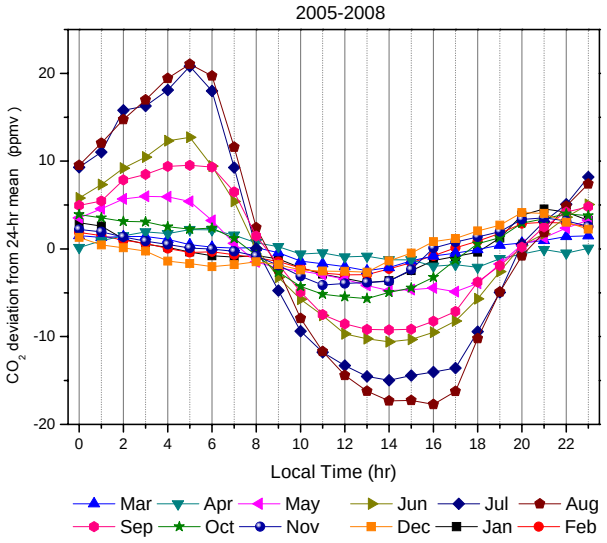

Fig. 3. Mean standardized diurnal variation of CO_2 by month at Miyun (2005–2008).

CO_2 is somewhat higher at night because surface sources are confined by a shallow boundary layer and stronger vertical mixing in the day brings down lower CO_2 air from aloft. The mean diel ranges in summer and winter were around 33 ppmv and 7 ppmv respectively. The diel range is largest in August, reaching approximately 39 ppmv on average.

3.1.2 Trends and seasonal variations

Although influenced somewhat by the frequency and timing of data gaps, annual summary statistics for CO_2 observed at Miyun (Table 1) show an average increase from 392.2 ppmv in 2005 to 400.4 ppmv in 2008, at an average rate of 2 ppmv/yr. Median mixing ratios increased at a similar rate. Substantial variability was observed for CO_2 at hourly time steps, as indicated by the range of observations listed in Table 1. The large short-term variations were attributed to the influence of anthropogenic pollution plumes, biospheric activity and synoptic weather conditions, as the site is located near urban and agriculture areas. The annual mean is approximately 3 ppmv higher than the median in each year, indicating that the distribution of hourly CO_2 was skewed toward the higher end.

Figure 4 presents the monthly mean CO_2 at Miyun compared with observations at several background stations of NOAA/ESRL (GLOBALVIEW-CO_2, 2009; Conway et al., 2009) and other agencies, including Mt. Waliguan (WLG; 36.29° N, 100.9° E, 3810 m a.s.l) in western China, Ulaan Uul (UUM; 44.45° N, 111.10° E, 914 m a.s.l) in Mongolia, Tae-ahn Peninsula (TAP; 36.73° N, 126.13° E, 20 m a.s.l) in South Korea, Niwot Ridge (NWR; 40.05° N, 120.58° W, 352 m a.s.l) and Wendover (UTA; 39.90° N, 113.72° W, 1320 m a.s.l) in the United States, and Terceira Island (AZR; 38.77° N, 27.38° W, 40 m a.s.l) in the Azores. These ERSL sites were selected because they are located either in/around China or are at about the same latitude as Miyun. CO_2 at Mauna Loa (MLO; 19.54° N, 155.58° W, 3397 m a.s.l) is included to represent the mean global CO_2 trend. Unlike the ESRL background stations, which are typically high elevation or coastal sites that are not influenced by local sources and vegetative activity, the Miyun site is situated within a heavily vegetated region and near major anthropogenic sources. These factors will strongly influence atmospheric CO_2 levels at Miyun. Monthly mean CO_2 mixing ratios observed at the Miyun site are typically more than 10 ppmv higher than those observed at the ESRL stations. The seasonal transition in CO_2 is not smooth at Miyun. Enhanced CO_2 levels are observed frequently in early summer (June) at Miyun, often of comparable magnitude to CO_2 levels in winter. This feature can be explained by frequent sampling of anthropogenic pollution exported from the Beijing urban area under the prevailing southwesterly winds associated with the East Asian summer monsoon.

The weekly averages of hourly CO_2 are presented in Fig. 5. All the data (i.e., 24-hour) are included in this figure and we will distinguish nighttime and daytime data in

Table 1. Descriptive statistics of CO_2 observation from 2005 to 2008.

	2005	2006	2007	2008
mean (ppmv)	392.17	397.02	399.62	400.35
median (ppmv)	389.31	394.89	396.17	397.59
min (ppmv)	350.75	349.30	343.66	352.57
max (ppmv)	478.21	481.59	488.77	467.92
Data completeness	78.0%	81.7%	92.6%	84.4%

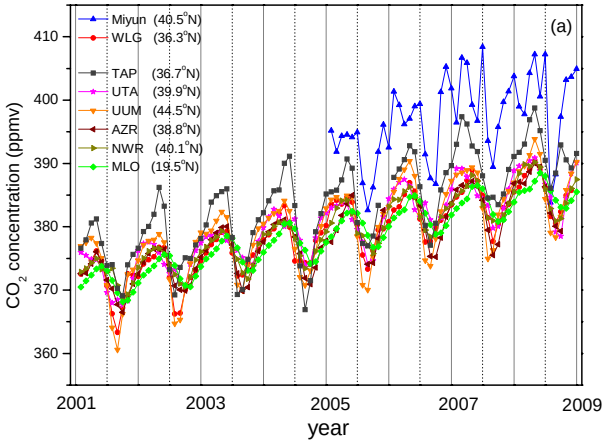

Fig. 4. Monthly mean CO_2 at Miyun site and several NOAA/ESRL sites. The solid gray lines denote January of each year, with the dotted gray lines indicating June.

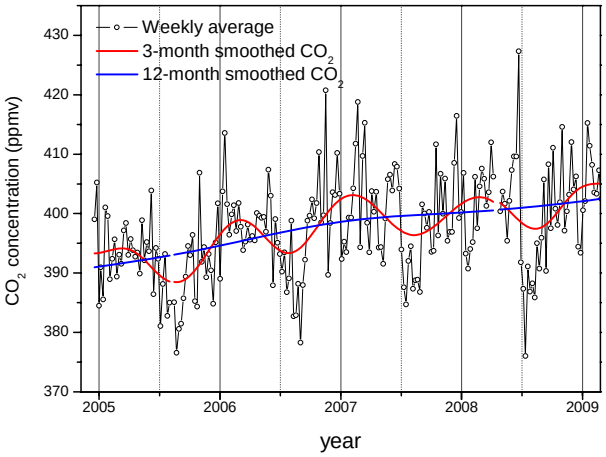

Fig. 5. Weekly mean CO_2 at Miyun from December 2004 to February 2009 (black line). The red and blue line is an FFT-filtered curve of the seasonal and annual variations, respectively. The thin solid gray lines denote January of each year, with the dotted gray lines indicating June.

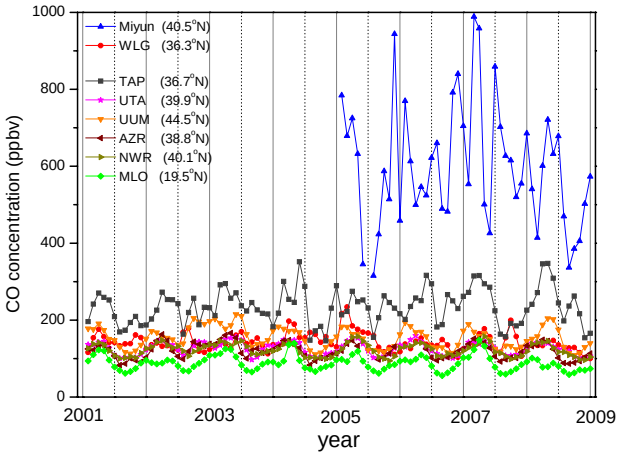

Fig. 6. Monthly mean CO at Miyun site and several NOAA/ESRL sites. The solid gray lines denote January of each year, with the dotted gray lines indicating June.

subsequent discussions. The weekly means ranged from 375 ppmv to 425 ppmv. From the weekly data, one can see clearly that the minima of CO_2 were observed in middle and late summer, the season with the strongest local photosynthetic uptake of CO_2 and lowest global background. Although high CO_2 in June is significant, the peaks occurred more frequently in winter when biological fluxes are only positive (i.e., release of CO_2 from respiration), strong temperature inversions trap emissions near the surface, and anthropogenic sources increase due to domestic heating. A fast Fourier transform (FFT) method (Thoning et al., 1989) was used to smooth out the weekly data in order to reveal the seasonal amplitude and annual rate of increase of CO_2 at Miyun. In the FFT filtering, the point window was selected as 13 (i.e., 13-week, roughly 3-month) and 52 (i.e., 12-month) to derive the seasonal (red line in Fig. 4) and annual (blue line in Fig. 4) variations respectively. The FFT filtering removes short-term variability and reveals the seasonal cycle of CO_2 similar to those found at the ESRL background sites: minima in summer, maxima in winter, and smooth transition in other seasons. The average seasonal amplitude of CO_2 (detrended) is 7.4 ppmv. The average rate of increase is 2.7 ppmv per year over the study period, similar to that reported by Cho et al. (2007). If nighttime (7 p.m.–7 a.m.) observations are excluded, the average seasonal amplitude (detrended) is 13.6 ppmv for daytime CO_2, and the average rate of increase is 2.5 ppmv per year over the study period. If only the afternoon observations (noon – 6 p.m.) are considered, the average seasonal amplitude (detrended) increased to 16.5 ppmv and the average rate of growth is 1.9 ppmv. The rate of increase appears to have slowed with time. Mixing ratios of CO_2 increased by approximately 4.0 ppmv from the beginning of 2005 to the beginning of 2006, 4.2 ppmv from 2006 to 2007, 1.4 ppmv from 2007 to 2008, and 1.2 ppmv from 2008 to 2009. Based on the energy statistics, Gregg et al. (2008) suggested that the rate of increase in CO_2 emissions from fossil fuel combustion and cement production in China slowed from 18% in 2004 to 8% in 2006. Although the relative decrease in the growth rate of emissions appears comparable to that of Miyun CO_2 concentrations, the timing when the change had occurred does not exactly match (2006 for emissions versus 2007 for Miyun CO_2). The regional impact of the emission reduction measures that reduced traffic or shut down industrial sectors implemented prior to, during, and after the 2008 Olympic Games in Beijing is expected to have large influence on emissions of CO_2 in 2007–2008 (to be discussed in Sect. 5). Atmospheric CO_2 observed at Miyun may reflect a combination of these factors.

3.2 CO_2-CO Correlation

CO is co-emitted with CO_2 from combustion sources, leading to a significant positive correlation between them when combustion is a significant source of observed CO_2. A summary of the monthly mean CO at Miyun is presented in Fig. 6 comparing with CO observations at the background stations listed above (Novelli and Masarie, 2010). Monthly mean CO ranged from 300 ppbv to 1000 ppbv with irregular seasonality. High CO levels indicate that regional pollution sources are frequently sampled at Miyun and will be reflected also in concurrent measurements of CO_2. Detailed analysis of CO seasonality at Miyun is given by Wang et al. (2010a).

Figure 7 presents the relationship between hourly CO_2 and CO means observed at Miyun, showing 2007 and 2008 data (Mar 2007 through Feb 2008) as examples. Considering the measurement uncertainty in both CO and CO_2 (Sect. 2), the

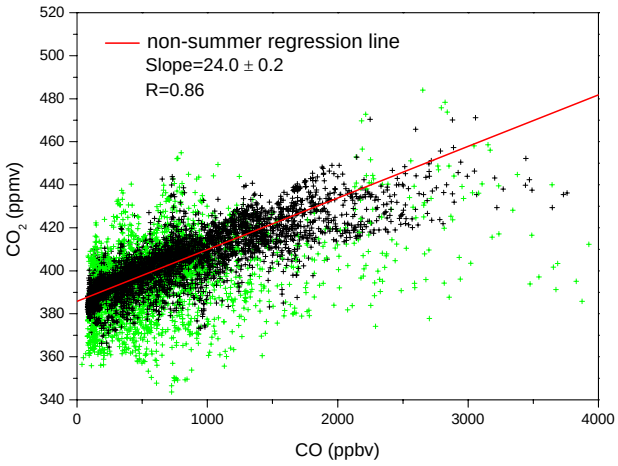

Fig. 7. CO_2-CO relationship observed at Miyun (March 2007–February 2008). Each data point represents hourly mean mixing ratios of CO (x-axis) and CO_2 (y-axis). The green crosses represent summertime observations. The correlation coefficient and slope shown in insert are derived from the reduced major axis method (see text). The red line is the regression line for non-summer observations.

two variables should be treated as symmetrical. Therefore, the reduced major axis method (Hirsch and Gilroy, 1984) was adopted to derive the correlations, instead of using the ordinary least square method. CO_2 and CO had strong correlation in the winter, indicating strong influences of combustion emissions on CO_2. The correlation coefficient was much smaller in the spring and fall, with correlation slopes similar to that observed in winter. As illustrated by the diel cycles, the CO_2 signal is dominated by the biosphere from May to September, with a maximum drawdown of 39 ppmv in daily CO_2 in the summer. Biospheric activity, however, has little impact on CO except for the CO source from in situ oxidation of biogenic hydrocarbons. The correlation between CO_2 and CO in the summer was insignificant (the summer data is highlighted by green crosses in Fig. 7). Excluding the summer data, the overall CO_2/CO correlation slope at Miyun was about 24 ppmv/ppmv during 2007–2008. Suntharalingam et al. (2004) derived the CO_2/CO ratio of 18 ppmv/ppmv from the TRACE-P aircraft measurements downwind of China in the spring of 2001. Han et al. (2009) derived the CO_2/CO ratio of 23 ppmv/ppmv in winter at an urban site in Beijing. The emission ratio of CO_2 to CO in 2000, derived from the bottom-up emission inventories of Streets et al. (2003) for CO_2 and Streets et al. (2006) for CO, was 15 mol/mol (mol/mol is equivalent to ppmv/ppmv) for the whole country and 14 mol/mol for provinces in northern China. More recent bottom-up studies on Chinese anthropogenic emissions by Zhang et al. (2009) for CO and Gregg et al. (2008) for CO_2 indicated that the emission ratio of CO_2 to CO in China was about 21 mol/mol in 2006.

In addition, non-combustion (biospheric) sources of CO_2 that are comingled with combustion sources over large spatial scales will contribute to observed CO_2-CO correlations because their variances are affected by the same atmospheric transport (Gloor et al., 2001; Folini et al., 2009). In particular, the overall respiration component from a densely populated urban area may be significant relative to combustion. Because respiratory CO_2 emissions by urban residents are collocated with urban combustion sources, respired CO_2 will be part of the urban plume and contribute to the observed CO_2/CO correlations. Based on per capita energy consumption and average human respiratory emissions, respiration by urban residents should add about another 2 mole CO_2 per mole of CO (supplementary material S.1). Respiratory CO_2 from soils and livestock is likely an important source of CO_2, but because these sources are spatially distinct from densely populated urban areas we expect the correlation between this CO_2 and CO to have a weaker correlation. Soil respiration in winter is likely minimized by cold temperatures and arid climate. Furthermore, sources of CO_2 and CO outside China may contribute to the observed CO_2/CO correlation at Miyun to the extent that neither gas is significantly perturbed by chemical reaction or surface exchange during transport. In Sect. 4, background trajectory analysis will be employed to segregate air masses representing regional emissions from northern China. The CO_2/CO correlation slopes for those observations will be compared with bottom-up emission estimates.

The magnitude of CO_2 variance driven by surface exchange with soils and vegetation exceeds the variance from combustion sources, hence CO_2:CO correlations are low in the summer. The correlation coefficient (R) between CO_2 and CO was 0.4 for the whole dataset in the summer of 2007. To distinguish between the relative contributions of anthropogenic emissions and biospheric activities to CO_2 during the period of active vegetation (summer), the correlation analysis was modified to account for diel patterns imparted by photosynthesis and respiration. The mean R for entire summer increased to about 0.5 when CO_2:CO correlation was computed separately for each hour of the day. Binning the data by both hour and month (3 month$\times$24 h) increases the average R above 0.6, though each data group was left with only about 30 data points. The separation by time of day and month is analogous to the CO_2-CO analysis by Potosnak et al. (1999) but without the added factor based on local CO_2 flux that would account for influence of temperature, solar radiation, water availability, and other factors that affect CO_2 uptake and emission, which reduced the summertime correlation coefficients below the values observed in winter. Nevertheless, compared to the overall correlation analysis, the grouping method by local time can provide useful information with statistical significance for the CO_2-CO relationship during warm seasons. The CO_2/CO slope observed at Miyun represents mainly the signature of urban emissions and the intercept depends on the initial condition set by global CO_2

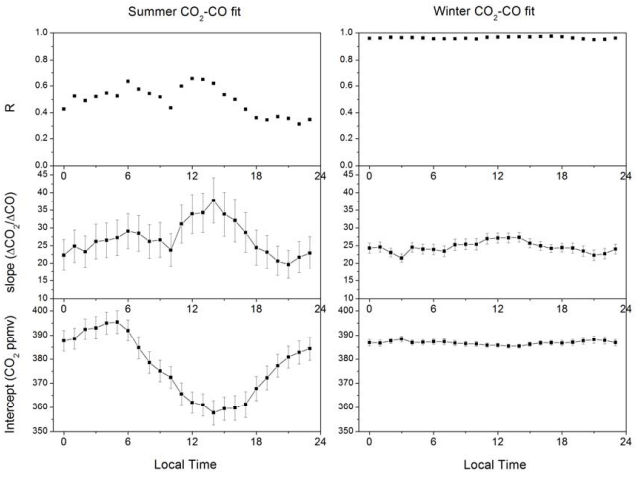

Fig. 8. The correlation coefficients (R), correlation slope (dCO_2/dCO), and intercepts of CO_2-CO regression at Miyun as a function of local time for summer (left) and winter (right), 2007.

distribution and non-CO related CO_2 sources and sinks. In what follows, the CO_2/CO correlation slope (or enhancement ratio) is denoted as dCO_2/dCO and correlation intercept as $CO_{2,i}$.

Figure 8 displays CO_2/CO correlation coefficient (R), dCO_2/dCO, and $CO_{2,i}$ as a function of local time in the summer (JJA) (left panel) and winter (DJF) (right panel) of 2007. Note that the intercept is not strictly interpreted as background CO_2 because background CO is not zero. The winter intercept remains largely constant within the 24 h, indicating that photosynthesis is dormant and respiratory CO_2 influence is more or less constant throughout the day. In contrast, the summer intercept shows a pronounced diel cycle, with a peak of 394.5 ppmv at 5 a.m. and a trough of 357.7 ppmv at 2 p.m. This reflects the uptake of CO_2 by photosynthesis during the day and release of it by respiration at night. The mean diurnal range of the intercepts is about 37 ppmv in the summer of 2007. The diurnal cycle of the intercepts is in phase with the diurnal cycle of CO_2 (33 ppmv) and with comparable amplitude, lending support to the correlation analysis by local time.

3.3 Background CO_2

We define "background" CO_2 as the level that would exist without influence of combustion sources, but still affected by net uptake or emission from biosphere. CO_2 mixing ratio at remote sampling sites (e.g. ESRL flask network) is not directly comparable with background defined here because it excludes the influence of regional and local biosphere. Although the Miyun site is located near major source regions, continuous high-frequency measurements of CO_2 and CO at the site allow for identification of background CO_2. The intercept of the CO_2-CO correlation ($CO_{2,i}$) was

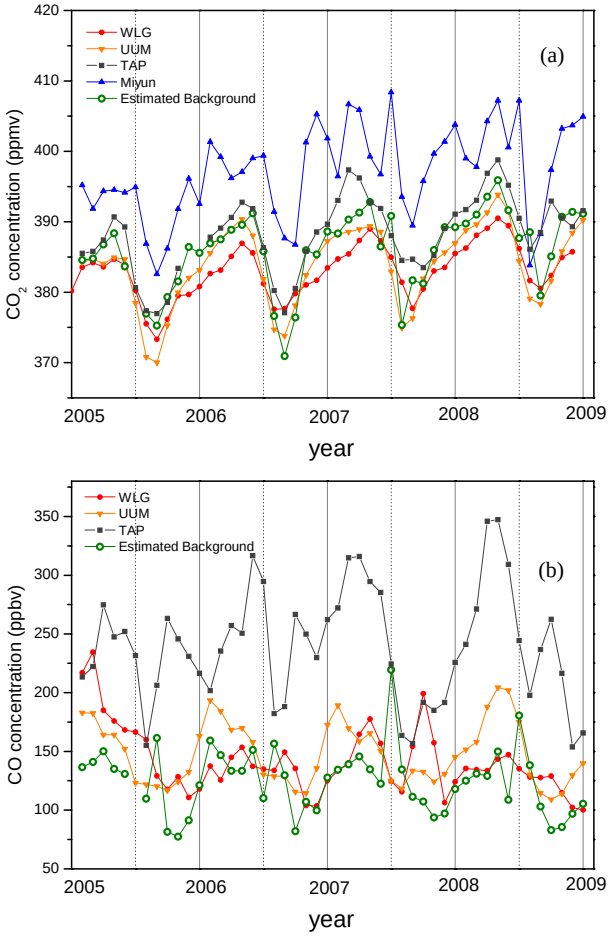

Fig. 9. Background CO_2 (a) and CO (b) derived at Miyun (green) compared to three ESRL sites (WLG, UUM, and TAP). The solid gray lines denote January of each year, with the dotted gray lines indicating June. Background CO_2 at Miyun is derived using Eq. (1). Background CO at Miyun is derived as the 5th percentile of observations in each month.

used to derive CO_2 at Miyun that has excluded the component correlated with the combustion tracer, CO. As discussed above, dCO_2/dCO and $CO_{2,i}$ are calculated by hours for each month, including the summer months. Averaging these hourly values by month gives the monthly mean intercepts and slopes. Because the intercept represents the expected value of CO_2 when CO mixing ratio is zero, but in reality there is a finite background CO, we use the 5th percentile of the CO distribution for each month as an estimate of background CO (CO_{bg}) and calculate the CO_2 mixing ratio at CO_{bg} by adding the product of dCO_2/dCO and CO_{bg} to the CO_2 intercept (denoted as $CO_{2,b}$ hereafter):

$$CO_{2,b} = CO_{2,i} + CO|_{5\%} \times dCO_2/dCO \quad (1)$$

Background CO_2 and CO estimated for each month is shown in Fig. 9a and b respectively in the context of monthly averages from ESRL data at several relevant sites. CO_{bg} at

Miyun is generally comparable with CO at the nearby background sites (Fig. 9b), except for a couple of months in summer due to data coverage issue or synoptic weather pattern not favorable for sampling of clean continental air masses. The uncertainty in CO_{bg} is estimated at about 20 ppbv, leading to 0.5 ppmv uncertainty in $CO_{2,b}$. The monthly mean $CO_{2,b}$ is about 11.1 ppmv lower than the overall monthly means at Miyun and exhibits regular seasonal cycles from year to year. Annual mean $CO_{2,b}$ is 386.1 ppmv at Miyun. Among the ESRL sites selected, UUM is located directly upwind of Miyun during the periods of northwesterly prevailing winds (UUM is 640 km northwest of Miyun), while WLG is a high-elevation site located on the Qinghai-Tibetan Plateau in western China with smaller seasonal variability in CO_2. TAP is a Korean site located downwind of Miyun with higher CO_2 all year around than other ESRL sites at similar latitude, likely due to the impact of regional pollution. Background CO_2 at Miyun shows seasonal cycles similar to monthly mean CO_2 observed at UUM. The differences between $CO_{2,b}$ at Miyun and CO_2 at the upwind UUM site, although confounded somewhat by air mass trajectories and exchange with the overlying free troposphere, can be interpreted in terms of whether the biosphere is a net source or sink of CO_2 in the region between the two sites. It can be seen from Fig. 9a that $CO_{2,b}$ at Miyun and CO_2 at UUM are largely overlapping with no substantial differences outside their uncertainties. This implies that the terrestrial biosphere over the region between the two sites is neither a very large sink nor a very large source of CO_2, which is consistent with the aridity and mountainous terrain with sparse vegetation between the sites

Monthly mean $CO_{2,b}$ and overall CO_2 (FFT-filtered) are compared in Fig. 10a. The difference between $CO_{2,b}$ and overall CO_2 reflects combustion contributions from local and regional sources in China that are correlated with CO. Mean CO_2 observed at the site exceeds $CO_{2,b}$ because local to regional sources influence the high values of CO_2 mixing ratio. Secular trends of $CO_{2,b}$ and CO_2 are presented in Fig. 10b. Annual growth of overall mean CO_2 is increasing by 2.7 ppm yr^{-1} while $CO_{2,b}$ is only increasing by 1.7 ppm yr^{-1}, which is not significantly different from the annual increase at the northern mid-latitude ESRL background stations (Fig. 4). The mean growth rate for CO_2 over the same period is 1.69 ppmv/yr at UUM, 1.37 ppmv/yr at WLG, and 1.6 ppmv/yr for all the northern mid-latitude ESRL stations shown in Fig. 4. Faster growth of mean CO_2, which depends on the middle and upper portion of the probability distribution of CO_2 observations that are affected by local and regional inputs, suggests relatively faster increase in the regional CO_2 sources in northern China than the global average. Indeed, the Carbon Dioxide Information Analysis Center (CDIAC) (Marland et al., 2007) reported an 8% increase in CO_2 emissions from fossil fuel consumption and cement production in China for 2006 compared to a 3.2% increase in global average emissions. This corresponds to a ratio of 2.5:1 (8/3.2) between China's emission growth rate and the world's in 2006, while Miyun data indicate a smaller ratio of 1.6: 1 (2.7/1.7) between regional CO_2 increases and global background. As this is a simple comparison, the discrepancy can be due to multiple factors such as the uncertainties in emission estimates, representativeness error of Miyun data for all of China, and the role of biosphere on regional and global CO_2.

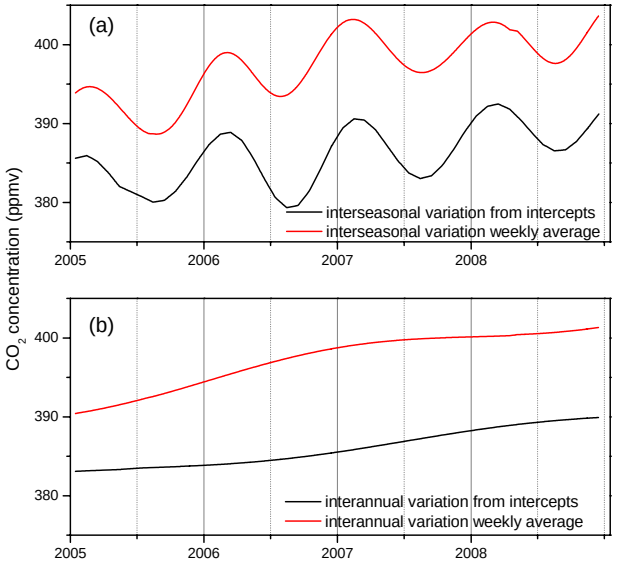

Fig. 10. The interseasonal (a) and annual (b) variations of CO_2 observed at Miyun (red) and background CO_2 (black) derived from the CO_2-CO correlation analysis.

4 Year-to-year variations in CO_2/CO ratio in winter

In this section, we examine year-to-year variations in dCO_2/dCO in wintertime at Miyun, as an indicator of combustion efficiency changes over northern China, during the study period extending five winters (Dec 2004 through Feb 2009). In this study, the winter season of a given year refers to a period of three months, from December of that year to February of the following year. For example, winter 2008 denotes Dec 2008 through Feb 2009.

We restrict our analysis to observations in winter for four reasons. First, the CO_2-CO correlation in this season is strongest suggesting that biospheric influence on CO_2 is less variable when photosynthesis is weak and the anthropogenic signature in CO_2 can be separated more robustly using CO as a tracer. Both CO_2 and CO have relatively longer atmospheric lifetimes in winter ($\sim$3 months for CO and $\sim$100 years for CO_2) because photosynthetic uptake of CO_2 is minimal in the north China region and CO oxidation is slowed. The correlations are better and representative of larger region because both gases have long enough lifetime

Table 2. The CO_2-CO correlation slope (dCO_2/dCO) and trend for winter observations at Miyun.

	Overall data[3]		CO-filtered data[2]		NCN air masses[3](CO filtered)	
Winter[1]	slope	error	slope	error	slope	error
2004	13.3	0.4	17.1	0.5	17.3	0.6
2005	21.8	0.4	23.5	0.6	23.8	0.9
2006	20.7	0.5	26.1	0.8	26.0	1.0
2007	25.7	0.4	27.7	0.8	28.6	1.1
2008	21.2	0.6	26.8	0.8	26.6	0.9
Change in mean slope from 2005–2006 and to 2007–2008	2.2 ± 0.5		2.5 ± 0.8		2.8 ± 0.9	

[1] Winter refers to a period of three months, from December of the listed year to February of the following year.
[2] The CO-filtered dataset refer to the data with CO levels between the 30th–90th percentiles. See text for details.
[3] CO_2-CO scatter plots for the overall data and for the NCN air masses are shown in supplementary material S.2 and S.3 respectively.

to be preserved during a day or two of transport as suggested by Gloor et al. (2001) of the tower transport time and footprint area. Second, the influence of biomass burning emissions is smallest in winter. Third, emissions associated with domestic heating, which contributes to a significant portion of fossil fuel consumption in China, are presented in winter observations. As a result, the winter CO_2-CO relationship should reflect more aspects of anthropogenic emissions compared with that of the other seasons. To avoid results that are dominated by specific local sources within a few km that are trapped in a shallow nighttime inversion layer, this analysis is restricted to daytime data when observations are more regionally representative (larger than tens of km). Fourth, vertical mixing is weaker in winter and local influences are accentuated. The observed CO levels and back trajectory cluster analysis were employed to segregate observational data that are representative of regional characteristics of emissions for northern China. The significance test (F-test) for the rate of change was conducted, with p (probability) less than or equal to 0.05 considered as statistically significant at 95% confidence interval (C.I.).

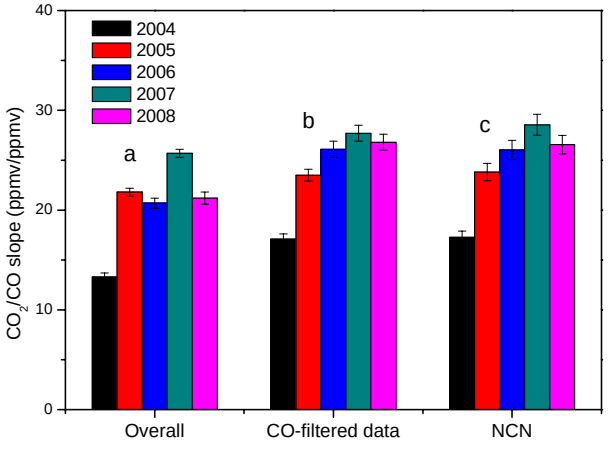

Fig. 11. The CO_2-CO correlation slope (dCO_2/dCO) for winter observations at Miyun. The slopes are evaluated for the overall dataset **(a)**, the CO-filtered dataset (with CO between the 30th and 90th percentiles) **(b)**, and the CO-filtered northern China air masses (NCN) **(c)**. The uncertainty bar is the uncertainty level of the slope calculated by RMA regression method.

4.1 Initial evaluation

A simple first step was to evaluate the overall dCO_2/dCO over the five winters before separating different air mass types, such as background and regional pollution. The overall dCO_2/dCO in each winter is summarized in Table 2 and Fig. 11a. The CO_2/CO slope increased from 13.3 ± 0.4 ppmv/ppmv in winter 2004 to 25.7 ± 0.4 ppmv/ppmv in winter 2007, and slightly decreased to 21.2 ± 0.6 ppmv/ppmv in winter 2008. The slope for winter 2004 was distinctly lower than the slopes for subsequent years. Measurements in winter 2004 had more gaps than subsequent winters due to instrument startup and restart period during the initial site setup. Examination of the scatter plots for individual years (supplementary material S.2) points to different patterns for the high and low CO data points, suggesting the CO-selective analysis described in the following section. It is inadequate to evaluate the overall slope using all the data and it is necessary to analyze the trend for selected air masses representing regional emissions from northern China.

The Miyun site is located on the edge of major source regions and there is a strong gradient in emission sources between the Beijing plain and the interior mountainous regions north of Miyun (Streets et al., 2006, Wang et al., 2008). The combustion tracer, CO, was selected as an indicator to differentiate air mass types in terms of pollution levels. Figure 12a shows the frequency distribution of CO observed in winter 2007 as an example. The distribution features a pronounced peak at about 160 ppbv. Based on the synoptic pattern in winter, this portion of the data reflects relatively

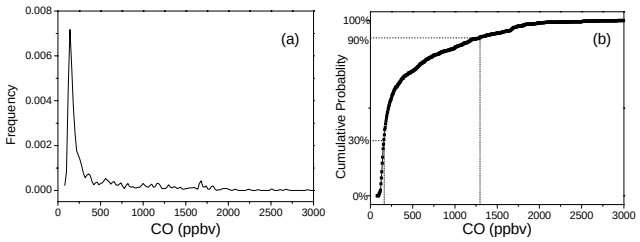

Fig. 12. Histogram **(a)** and cumulative probability distribution **(b)** of daytime CO mixing ratios in winter 2007 (December 2007 through February 2008).

clean background continental air masses from the north. The long tail toward very high CO (>1000 ppbv) represents urban pollution plumes and local rural pollution with high levels of CO. The distribution of CO in winters of other years is similar. Based on the cumulative probability distribution of CO (Fig. 12b), the wintertime dataset can be divided roughly into three subsets using CO as a criterion: below the 30th percentile, between the 30th and 90th percentile, and above the 90^{th} percentile of CO. The dataset with CO below the 30th percentile all had CO levels less than 160 ppbv, typically continental background air masses from the north. The dataset with CO exceeding the 90th percentile is high in both CO_2 (>385 ppmv) and CO (>1000 ppbv), but with lower CO_2/CO slopes (about 3.3 ppmv/ppmv) compared with the other datasets, indicating the dominance by local sources (e.g. biofuel combustion in the nearby village) that typically have low combustion efficiency and are trapped in a shallow inversion layer (Streets et al., 2006). The dataset with CO between the 30th and 90th percentile is selected to represent the regional signature of CO_2 and CO over northern China with a well-mixed blend of sources. Hereafter, we refer to this subset of the dataset as the China regional dataset or CO-filtered dataset. The CO_2-CO correlation slopes for the China regional dataset are summarized in Table 2 and Fig. 11b. As for the overall slopes, the CO_2/CO slope in CO-filtered data was significantly lower in 2004 than in subsequent years. The CO_2/CO slope increased from 17.1 ± 0.5 ppmv/ppmv in winter 2004 to 23.5 ± 0.6 ppmv/ppmv in winter 2005. The slope continued to increase from 2005–2007 and dropped somewhat in 2008.

4.2 Air mass groups using cluster analysis

A more robust method to identify influential source regions is to understand transport paths of air masses to the site through back trajectory modeling. The HYSPLIT (Hybrid Single-Particle Lagrangian Integrated Trajectory) model (version 4.9) (http://www.arl.noaa.gov/HYSPLIT.php) (Draxler and Hess, 1998) was employed in this study to calculate backward trajectories of observations in winter. The meteorological data employed to calculate the back trajectories are GDAS reanalysis data at $1^\circ \times 1^\circ$ spatial resolution. The back trajectories are calculated twice a day, at 1000 h and 1500 h local time respectively, with the initial height of 6m and time steps of 1 h. To show the regional effect, 72-h (3-day) back trajectories are calculated for each day of the five winters (2004–2008). This corresponded to 722 back trajectories, which are classified into four air-mass groups (Fig. 13a–d) based on cluster analysis (Dorling et al., 1992). Mean altitudes of the four groups are displayed in Fig. 13e. As a result of the influence of the Siberian High (a massive high pressure system on the Eurasian terrain driving the northwesterly winter monsoon) on synoptic patterns in winter, the majority of the 3-day back trajectories originated from the northwest and was typically confined below 2 km. The four air-mass groups are: Central Eastern Siberia (CES) (13a), Aged Continental (AC) (13b), Northwest China (NWC) (13c), and North China Plain (NCP) (13d). The CES air masses originated in the relatively clean central Eastern Siberian region (east of 90° E and north of 55° N) and can be considered background continental air. The AC air masses originated in central Asia west of 90° E and were transported over long distances before arriving at the site. Newell and Evans (2000) suggested that this type of air mass is responsible for influxes of aged pollution from Europe to China. The NWC air masses originated in northwestern China and Mongolia (west of 100° E), and were transported eastward to the site with the majority of their courses in China. Most of the NCP air mass originated and traveled within northern China. The CES, AC, NWC, and NCP groups, respectively, account for 22%, 20%, 17%, and 39% of all air masses calculated for the four winters. A small portion (<2%) of the trajectories is of an unclassified type. The average fractional time that each group of air masses spends below 500 m in China is 21%, 22%, 46%, and 69% for the CES, CA, NWC, and NCP groups, respectively. In the following discussion, the NWC and NCP air masses were grouped into one "North China" (NCN) group, in part because the two air mass groups spent a significant fraction of their travel times within the northern China boundary layer before arriving at Miyun and had similar mixing ratios of CO_2 and CO. The NCN group is the predominant air mass group in the winter, most representative of surface fluxes (sources or sinks) of CO and CO_2 in northern China.

Although trajectories are known to be good indicators of large-scale flow, there are uncertainties in the trajectory model calculation. The relatively coarse resolution of the meteorology data (both spatial and temporal) indicates that the model cannot resolve the mesoscale transport, and especially the influence of local mountains. Therefore, we impose an additional constraint when examining the chemical characteristics of air masses by groups. Instead of using all the data, only the CO-filtered dataset discussed above (i.e., with CO between the 30th and 90th percentiles) are segregated into the four air mass groups. That is, we exclude the relatively clean air masses not representative of Chinese emissions as well as the heavily-polluted air masses

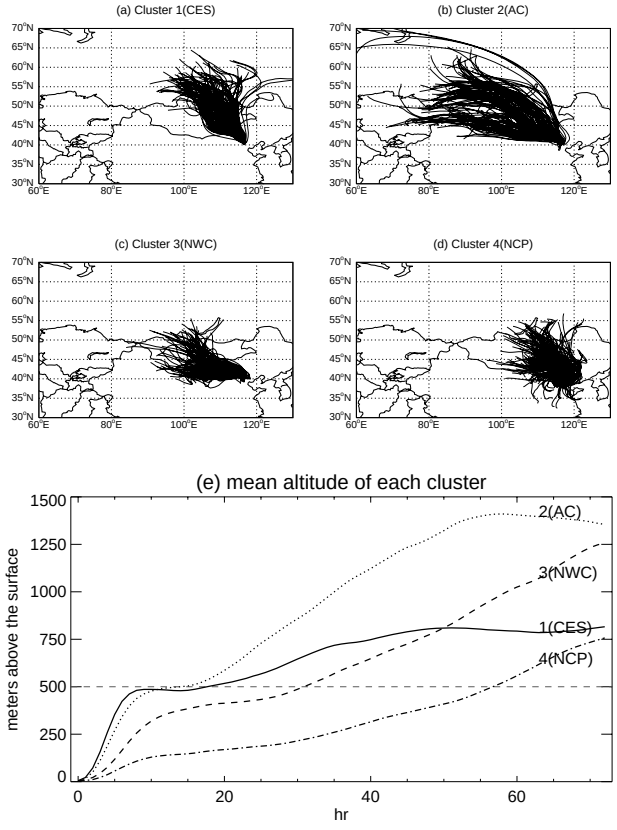

Fig. 13. Back trajectories for wintertime observations at Miyun (2004–2008) by clusters: Central East Siberia (CES) **(a)**, Aged Continental (AC) **(b)**, Northwest China (NWC) **(c)**, and North China Plain (NCP) **(d)**. The mean altitude of each cluster is shown in **(e)**.

influenced by local emissions and concentrated urban pollution plumes, both of which cannot be resolved by the back trajectory model. In what follows, air mass groups refer to the CO-filtered dataset instead of the whole dataset, unless stated explicitly. In Sect. 4.3, we will examine the sensitivity of our results if the whole dataset is segregated by air mass groups.

Table 3 summarizes mean CO_2, CO, and their relationship for the three air mass groups averaged over the five winters. As the CO-filtered dataset excludes the relatively clean air masses with CO less than the 30th percentile, the CES group accounts for only 12% of the CO-filtered data. The NCN group is the predominant group in the CO-filtered dataset, accounting for 69%. This group has the highest CO mixing ratios (666 ± 104.4 ppbv) and CO_2 mixing ratios (400 ± 4.4 ppmv), followed by the AC group and CES group. As expected of background air, the correlation between CO_2 and CO for the CES group is weaker than those of the AC or NCN groups. The difference in chemical composition of the three air mass groups is consistent with the expected gradients based on cluster analysis of air mass origins, lending support to the method adopted here.

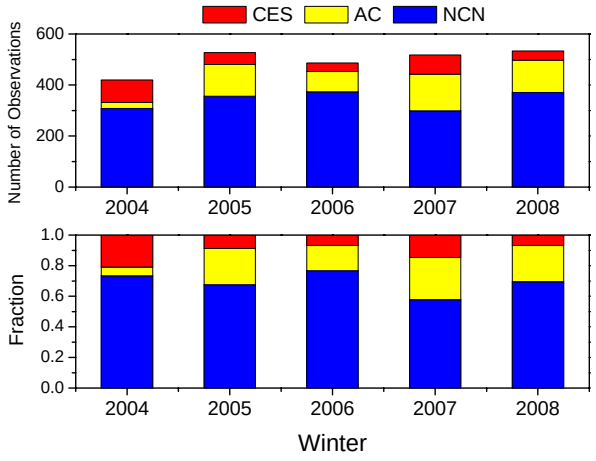

Fig. 14. (a) The number of observations in each winter by clusters; **(b)** The fraction of each cluster in total observations in each winter.

Figure 14 summarizes the number of CO_2-CO data pairs in each air mass group (14a) and their fractional contribution to the total number of CO-filtered observations (14b) for each winter. The total number of observations is comparable between winters 2005 and 2008, but lower in winter 2004 because of measurement gaps associated with instrument startup during the initial site setup period. The NCN group is the predominant group in each winter, consisting of more than 300 data pairs and accounting for 55%–75% of the total observations. For the CES and AC group, however, the year-to-year variations in the number of data points are more significant and the changes in dCO_2/dCO was not conducted for these groups. We examine next the variability in dCO_2/dCO for the NCN group.

4.3 CO_2/CO ratio for NCN air masses

The year-to-year changes in wintertime dCO_2/dCO for the NCN air mass group are summarized in Fig. 11c. The correlation slope, dCO_2/dCO, for the NCN air mass group increased from 17.3 ± 0.6 ppmv/ppmv in winter 2004 to 28.6 ± 1.1 ppmv/ppmv in winter 2007. It dropped somewhat to 26.6 ± 0.9 ppmv/ppmv in winter 2008. A linear fit of the five data gives an annual rate of increase of 2.61 ppmv/ppmv/yr ($p = 0.05$). When the whole dataset of NCN air masses was considered (i.e., without the CO filtering), the rate of increase in dCO_2/dCO was estimated at 2.64 ppmv/ppmv/yr ($p = 0.13$) over the five winters, comparable to the results above but with lower p-value. As background air masses low in CO are not representative of Chinese emissions and thus not expected to show a trend in the CO_2/CO ratio, including them in the trend analysis reduces the overall statistical significance. As discussed above, the data gaps due to instrument startup in winter 2004 may have introduced systematic errors in dCO_2/dCO for 2004.

Table 3. Mean CO_2, CO, and their relationship for each air mass group (CO-filtered) over the five winters (2004–2008).

Cluster	Share (%)	Mean CO_2 (ppmv)	Mean CO (ppbv)	Intercept (ppmv)	Slope (ppmv/ppmv)	R
CES	12	392.4	284.5	383.1 ± 3.7	33.1 ± 4.6	0.79
AC	19	396.3	496.6	385.0 ± 2.2	23.0 ± 6.7	0.93
NCN	69	400.2	666.1	384.2 ± 3.5	24.4 ± 4.4	0.94

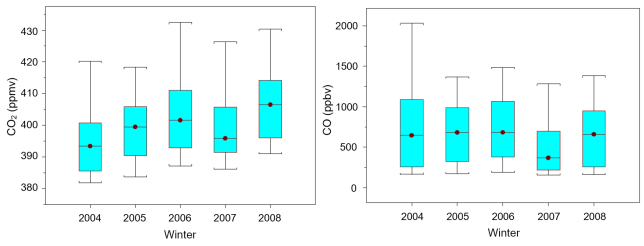

Fig. 15. Box plots of CO_2 **(a)** and CO **(b)** observations for the NCN air mass group at Miyun in winter, 2004–2008.

When winter 2004 was not included, the rate of increase in dCO_2/dCO reduced by 30%, to 1.6 ppm/ppm/yr ($p = 0.15$) for the NCN group, suggesting that the small dCO_2/dCO in winter 2004 has exerted a large impact on trend calculation above. Nevertheless, the increase in dCO_2/dCO from winter 2006 to winter 2007 is significant (2.6 ± 1.4 ppmv/ppmv), whereas the difference between other adjacent years is less significant. Therefore, we averaged dCO_2/dCO before winter 2007 (excluding winter 2004) and after winter 2007. Mean dCO_2/dCO was 27.6 ± 0.71 ppmv/ppmv for winters 2007–2008, compared to 24.8 ± 0.68 ppmv/ppmv for winters 2005–2006. The increase in mean dCO_2/dCO from winters 2005-2006 to winters 2007–2008 was 2.8 ± 0.9 ppm/ppm or roughly 11%.

Analysis of the year-to-year changes in CO_2 and CO of the NCN air masses separately (Fig. 15) suggested that the rate of increase in dCO_2/dCO was caused primarily by decreases in CO in 2007–2008 compared with 2005–2006, offsetting the effect of slowing CO_2 increases during the same period. Mean CO of the NCN air masses in the winter decreased at a rate of about -42.5 ppbv/yr ($p = 0.25$), although the trend is not statistically significant due to large variability in CO observed at Miyun. Large decreases in both CO and CO_2 were observed in winter 2007. Mean CO was lower by 230 ppbv and CO_2 by 3 ppmv compared to winter 2006. This was likely associated with the pollution reduction measures implemented in preparation for the 2008 Summer Olympics and Paralympics Games in Beijing. According to the plans listed by the Beijing municipal government (http://www.bjepb.gov.cn/bjhb/publish/portal0/tab151/info9190.htm, read 10 Dec, 2009), a number of highly polluting and energy inefficient cement, coking, steel, petrochemical, and power plants in Beijing had been relocated or closed off by the end of 2007. Inefficient small boilers and coal stoves for domestic heating were also replaced. These policies were implemented in stages before the actual Games, in contrast to the more temporary policies instituted during the two months of the Games that will be discussed in Sect. 5. It is estimated that approximately 50% of the industrial boilers were closed before December 2007 after the implementation of the 13th stage of emission control policies planned by the Beijing Environmental Protection Bureau (Wang et al., 2010b). Observations of CO_2 and CO at Miyun in winter 2007 (Dec 2007 through Feb 2008) suggest that these emission reduction measures had indeed become effective by early 2008, leading not only to reductions in pollution levels, but also reductions in overall energy consumption and increases in combustion efficiency as indicated by changes in CO_2 and dCO_2/dCO respectively. Mean CO in winter 2008 was higher than winter 2007, probably due to different transport patterns as indicated in the different fraction of NCN air masses between the two winters (Fig. 14), but lower than winter 2006 and before, suggesting that some but not all of the emission reduction measures associated with the 2008 Olympics had led to permanent reduction of pollution levels. Examples of the permanent measures are replacing inefficient residential boilers and stoves, while temporary shutdown of industrial boilers before the Games only had a short-term effect on CO. This will be further discussed in the next Section and Table 5.

As discussed above, the NCN air mass group is the predominant group in winter and most representative of regional emissions from northern China. The significant increase in the CO_2/CO correlation slope in this group of air masses from 2005–2006 to 2007–2008 suggests that the emission ratio between CO_2 and CO over northern China may have increased during the study period. As CO is a tracer of inefficient combustion, the increase in the emission ratio of CO_2 to CO indicates improvement in combustion efficiency over northern China. The emission reduction measures associated with the 2008 Beijing Olympics had resulted in not only reductions in pollution levels, but also increases in overall combustion efficiency over north China.

The CO_2/CO correlation slope for the NCN group was 26.0 ± 1.0 ppmv/ppmv in winter 2006. As discussed above, the emission ratio between CO_2 and CO for China was 21 mol/mol in 2006 as derived from bottom-up inventories of anthropogenic emissions of CO_2 (Gregg et al., 2008) and CO (Zhang et al., 2009). Observationally based estimates of CO_2/CO are sensitive to all sources of CO_2 and CO that have statistical correlation. Both co-emitting sources and adjacent but separate sources that become correlated because of transport are included. In particular CO_2 from respiration by residents of dense urban areas will be correlated with other urban emissions including vehicles and boilers when the urban plume is sampled downwind, leading to an enhanced CO_2/CO ratio relative to bottom-up inventories that only account for combustion sources. Indeed the observed CO_2/CO ratio at Miyun (26 ppmv/ppmv) is 25% higher than the bottom-up estimate of CO_2/CO emission ratio (21 ppmv/ppmv), which is consistent with a contribution of respired CO_2 from urban residents. However, the enhancement exceeds the ~10% expected from a simple estimate based on per capita energy use and average CO_2 respiration discussed above. Additionally, the difference between inventory and observed ratios may indicate the presence of seasonality and spatial variability that generate differences when annual national means are compared to a site-specific winter-only value. Another explanation is that the bottom-up inventories either underestimated Chinese combustion emissions of CO_2 or overestimated emissions of CO. Future analysis of the discrepancy will combine higher resolution transport model and detailed inventories of all CO_2 and CO sources to simulate the CO_2 and CO correlations at Miyun and be discussed in a subsequent manuscript.

5 Case study: CO_2/CO ratio during the 2008 Beijing Olympics

To improve air quality during the 2008 Olympics (8–24 August) and the Paralympic Games (9–17 September), aggressive emission reduction measures were implemented temporarily for about two months in Beijing and its surrounding regions, including Tianjin municipality, Hebei, Inner Mongolia, Shanxi, and Shandong. Starting 1 July, 2008, all vehicles that failed to meet the Euro 1 standards for exhaust emissions were banned from traveling on Beijing roads. Between July 20 and September 20, private vehicles in Beijing were only allowed to travel on odd or even numbered days according to their plate number. Companies were required to take strict control measures by the end of June to ensure that their pollution did not exceed permitted levels. Wang et al. (2009), through comparative analysis of long-term Miyun observations before and during the Olympics, suggested that the emission reduction measures during the Olympics were effective in reducing pollutant concentrations such as O_3, CO, SO_2, and NO_x in Beijing. In this section, observations of CO_2 and its correlation with CO at the site during the Olympics are presented as a case study to examine the effect of the pollution reduction measures on energy consumption and combustion efficiency.

Most of the emission control measures were in effect from July until the end of September in 2008. To minimize the impact of the biosphere on CO_2, we focus on CO_2 and CO observations in September instead of those in July or August. The monthly average CO mixing ratio in September was the lowest in 2008 among the four years (Wang et al., 2009). Table 4 compares mean CO_2-CO correlation slopes with uncertainties for each September over the four years. The CO_2-CO correlation slopes were calculated as the averages of the hourly CO_2-CO slope for each month. The CO_2-CO slope in September 2008 was 46.4 ± 4.6 ppmv/ppmv, higher by about a factor of two than the range of 23–29 ppmv/ppmv in September 2005–2007. The increase in the CO_2/CO ratio was driven primarily by the decrease in CO, resulting from the temporary ban of vehicles, which have low combustion efficiency compared to most other fossil energy uses, from the road. Mean mixing ratios of CO_2 increased by 1.6 ppmv in September 2008 as compared to September 2007, consistent with the mean annual growth in CO_2 observed at the site that is driven by rising global background. The increase in the CO_2/CO ratio in September 2008 indicates that emission reduction measures implemented during the Games period resulted in significant improvement in overall combustion efficiency.

Table 5 compares the CO_2-CO correlation slopes for October, November, and December in 2008 with the average slopes during the corresponding months in 2005–2007. The CO_2-CO correlation slopes were calculated as the averages of the hourly CO_2-CO slope for each month. The CO_2/CO correlation slope declined after the Olympics, as the temporary emission reduction measures such as traffic controls were relaxed. However, dCO_2/dCO of October, November and December 2008 were still higher than previous years, implying that the emission reduction measures associated with the Olympics had long lasting effects on improved combustion efficiency in Beijing as discussed above.

6 Concluding remarks

We have analyzed temporal variations of CO_2 and its correlation with CO at Miyun, a rural site near Beijing, based on continuous measurements over a period of 51 months (Dec 2004 through Feb 2009). The site is located 100 km northeast of Beijing's urban center, well situated to measure both the urban pollution and the relatively clean continental background. Compared with CO_2 mixing ratios reported by ESRL for background sites at similar latitudes, monthly mean CO_2 mixing ratios at Miyun are 10 ppmv higher on average and exhibit irregular seasonal cycles, reflecting influence from local and regional sources and sinks.

Table 4. Mean CO_2 and CO mixing ratio and their correlations for September, 2005–2008. CO_2-CO scatter plots for September observations in individual years are shown in supplementary material S.4.

		2005	2006	2007	2008
CO (ppbv)	Mean	586.80	482.14	615.10	385.25
	Median	450.52	441.49	566.09	303.03
	25-percentile	124.55	180.27	309.22	179.68
	75-percentile	821.15	640.87	813.32	553.13
CO2 (ppmv)	Mean	390.01	386.82	395.76	397.41
	Median	389.33	386.05	394.02	397.12
	25-percentile	381.81	377.63	385.85	385.94
	75-percentile	396.80	394.7	402.78	407.18
dCO_2/dCO (ppmv/ppmv)		23.9 ± 8.4	27.7 ± 10.0	28.8 ± 5.6	46.4 ± 4.6
R		0.84 ± 0.05	0.65 ± 0.11	0.56 ± 0.14	0.76 ± 0.06

Table 5. dCO_2/dCO for October, November, and December, 2005–2008. CO_2-CO scatter plots for observations in individual years are shown in supplementary material S.4.

dCO_2/dCO (ppmv/ppmv)	Oct	Nov	Dec
Average for 2005–2007	24.8 ± 4.3	21.5 ± 5.2	23.2 ± 2.4
2008	38.7 ± 5.5	30.9 ± 2.7	29.6 ± 1.4

The overall CO_2-CO correlation is significant for winter months, but degraded by the influence of photosynthesis and respiration in the growing season. However, CO_2-CO correlations segregated by local time can still provide useful information with statistical significance for the CO_2-CO relationship during the growing season. The intercept ($CO_{2,i}$) defines a component in total CO_2 that is independent of CO, combining transport from background, and net effect of biogenic sources and sinks as well as any combustion sources that are CO free. The diurnal range of $CO_{2,i}$ has an amplitude near zero in the winter when both combustion and biotic emissions are relatively constant. The amplitude of diurnal cycle for $CO_{2,i}$ is 38 ppmv in the summer when the magnitude of surface CO_2 exchange is large and the sign changes between night and day.

Background CO_2 levels ($CO_{2,b}$) at Miyun as derived from $CO_{2,i}$ are comparable with CO_2 levels observed at UUM, an upwind background site 640 km northwest of Miyun, in terms of both magnitude and seasonality. The difference can be used as a diagnostic for the net source/sink of CO_2 across Mongolia and China north of the Miyun site. The difference between $CO_{2,b}$ and overall CO_2 at Miyun reflects combustion contributions from local and regional sources in north China. Mean CO_2 observed at the site exceeds $CO_{2,b}$ because local to regional sources influence the high values of CO_2 mixing ratio. Annual growth of overall mean CO_2 is increasing by 2.7 ppm yr^{-1} while $CO_{2,b}$ is only increasing by 1.7 ppm yr^{-1}. The mean growth rate for CO_2 for the northern mid-latitude ESRL background stations is 1.6 ppm yr^{-1} over the same period. Faster growth of mean CO_2suggests relatively faster increase in the regional CO_2 sources in northern China than the global average. Bottom-up studies of CO_2 emissions (Marland et al., 2007) suggested annual increase in Chinese fossil CO_2 emissions is a factor of 2.5 ($8/3.2 = 2.5$) larger than the global average in 2006. The Miyun data, however, suggests a much smaller difference of 1.6 ($2.7/1.7 = 1.6$). As this is a simple comparison, the discrepancy can be due to multiple factors such as the uncertainties in emission estimates, representativeness error of Miyun data for whole China, and the role of biosphere on regional and global CO_2.

For the group of air masses coming from the northern China boundary layer as segregated using back trajectory analysis (NCN air masses), mean winter CO_2/CO correlation slopes (dCO_2/dCO) increased by 2.8 ± 0.9 ppmv/ppmv or 11% from 2005–2006 to 2007–2008. The increase in dCO_2/dCO was caused primarily by decrease in CO over the study period, offsetting the slowing down of CO_2 growth rate between 2007–2008. As CO is a tracer of inefficient combustion, the observed trend of increase in dCO_2/dCO at Miyun suggests improvement in overall combustion efficiency over northern China during the study period. The increase in dCO_2/dCO resulted from pollution reduction measures associated with the 2008 Summer Olympics and Paralympic Games in Beijing. On one hand, some measures such as the gradual phasing out of inefficient and polluting factories and boilers were implemented in stages in advance of the actual Games, leading to the changes in dCO_2/dCO observed for winter 2007–2008. On the other hand, there were aggressive, temporary policies instituted during the two months of the Games, such as traffic bans. We found that the temporary pollution reduction measures resulted in increases in dCO_2/dCO by a factor of two in September 2008, relative to the same months in 2005–2007.

The CO_2/CO correlation slope for the NCN group was 26.0 ± 1.0 ppmv/ppmv in winter 2006, 25% higher than the bottom up estimate of CO2/CO emission ratio for China (21 ppmv/ppmv). In part this difference may arise because national inventories averaged for a whole year are being compared to observationally based emission inventories for a smaller sub-region and single (winter) season. CO_2 from respiration by residents of dense urban areas will be correlated with other urban emissions including vehicles and boilers when the urban plume is sampled downwind, leading to a 10% enhancement in CO_2/CO ratio relative to bottom-up inventories that only account for combustion sources. This suggests that the site observations represent an overall "urban respiration" source. To address the discrepancy, future analysis involving higher resolution transport models and detailed inventories of all CO_2 and CO sources is needed to simulate the observed CO_2 and CO correlations.

Supplementary material related to this article is available online at: http://www.atmos-chem-phys.net/10/8881/2010/acp-10-8881-2010-supplement.pdf.

Acknowledgements. This research was supported by the National Science Foundation, grant ATM-0635548, and funds from the Harvard University Smeltzer Fund and an anonymous private foundation. Y. X. Wang was supported by the National High Technology Research and Development Program of China (Grant No. 2009AA122005) and by Tsinghua University Initiative Scientific Research Program. The authors thank A. E. Andrews and another anonymous reviewer for their helpful comments.

Edited by: C. Gerbig

References

Andreae, M. O. and Merlet, P.: Emission of trace gases and aerosols from biomass burning, Global Biogeochem. Cy., 15, 955–966, 2001.

Bakwin, P. S., Hurst, D. F., Tans, P. P., and Elkins, J. W.: Anthropogenic sources of halocarbons, sulfur hexafluoride, carbon monoxide, and methane in the southeastern united states, J. Geophys. Res.-Atmos., 102, 15915–15925, 1997.

Bakwin, P. S., Tans, P. P., Hurst, D. F. and Zhao, C. L.: Measurements of carbon dioxide on very tall towers: results of the NOAA/CMDL program, Tellus, 50B, 401–415, 1998.

Bishop, G. A., McLaren, S. E., Stedman, D. H., Pierson, W. R., Zweidinger, R. B., and Ray, W. D.: Method comparisons of vehicle emissions measurements in the Fort McHenry and Tuscarora Mountain Tunnels, Atmos. Environ., 30(12), 2307–2316, 1996.

Bishop, G. A. and Stedman, D. H.: A decade of on-road emissions measurements, Environ. Sci. Technol. 42, 1651–1656, 2008.

Chen, D., Wang, Y., McElroy, M. B., He, K., Yantosca, R. M., and Le Sager, P.: Regional CO pollution and export in China simulated by the high-resolution nested-grid GEOS-Chem model, Atmos. Chem. Phys., 9, 3825–3839, doi:10.5194/acp-9-3825-2009, 2009.

Cho, C. H., Kim, J. S., and Yoo, H. J.: Atmospheric carbon dioxide variations at Korea GAW center from 1999 to 2006, J. Korean Meteorol. Soc., 43, 359–365, 2007.

Conway, T. J., Lang, P. M., and Masarie, K. A.: Atmospheric Carbon Dioxide Dry Air Mole Fractions from the NOAA ESRL Carbon Cycle Cooperative Global Air Sampling Network, 1968–2008, Version: 2009-07-15, Path: ftp://ftp.cmdl.noaa.gov/ccg/co2/flask/event/, 2009.

Dang, A. R., Shi, H. Z., and He, X. D.: Dynamic variation of land use based on 3S technology, Journal of Tsinghua University (Science and technology), 43, 1408–1411, 2003.

Daube, B. C., Boering, K. A., Andrews, A. E., and Wofsy, S. C.: A high-precision fast-response airborne CO_2 analyzer for in situ sampling from the surface to the middle stratosphere, J. Atmos. Ocean. Technol., 19(10), 1532–1543, 2002.

Draxler, R. R. and Hess, G. D.: An overview of the HYSPLIT 4 modelling system for trajectories, dispersion, and deposition, Austral. Meterol. Mag., 47, 295–308, 1998.

Dorling, S. R., Davies, T. D., and Pierce, C. E.: Cluster-analysis – a technique for estimating the synoptic meteorological controls on air and precipitation chemistry – method and applications, Atmos. Environ., 26, 2575–2581, 1992.

Fan, SM, TL Blaine, JL Sarmiento: Terrestrial carbon sink in the Northern Hemisphere estimated from the atmospheric CO_2 difference between Mauna Loa and the South Pole since 1959, Tellus, 51B, 863–870, 1999

Folini, D., Kaufmann, P., Ubl, S., and Henne, S.: Region of influence of 13 remote European measurement sites based on modeled carbon monoxide mixing ratios, J. Geophys. Res., 114, D08307, doi:10.1029/2008JD011125, 2009.

Fung, I. Y., Tucker, C. J., and Prentice, K. C.: Application of advanced very high-resolution radiometer vegetation index to study atmosphere-biosphere exchange of CO_2, J. Geophys. Res.-Atmos., 92, 2999–3015, 1987.

GLOBALVIEW-CO_2: Cooperative Atmospheric Data Integration Project – Carbon Dioxide. CD-ROM, NOAA ESRL, Boulder, Colorado (Also available on Internet via anonymous FTP to ftp.cmdl.noaa.gov, Path: ccg/co2/GLOBALVIEW), 2009.

Gloor, M., Bakwin, P., Hurst, D., Lock, L., Draxler, R., and Tans, P.: What is the concentration footprint of a tall tower?, J. Geophys. Res., 106(D16), 17831–17840, 2001.

Gregg, J. S., Andres, R. J., and Marland, G.: China: Emissions pattern of the world leader in CO_2 emissions from fossil fuel consumption and cement production, Geophys. Res. Lett., 35, L08806, doi:10.1029/2007GL032887, 2008.

Han, S., Kondo, Y., Oshima, N., Takegawa, N., Miyazaki, Y., et al.: Temporal variations of elemental carbon in Beijing, J. Geophys. Res., 114, D23202, doi:10.1029/2009JD012027, 2009.

Hirsch, R. M. and Gilroy, E. J.: Methods of fitting a straight-line to data - examples in water-resources, Water Resour. Bull., 20, 705–711, 1984.

Jin, F. and Lee, D.: Continuous Monitoring and the Source Identification of Carbon Dioxide at Three Sites in Northeast Asia During 2004–2005, Advanced Environmental Monitoring, 77–89, 2008.

Keeling, C. D., Bacastow, R. B., Bainbridge, A. E., Ekdahl, C. A., Guenther, P. R., Waterman, L. S., and Chin, J. F. S.: Atmospheric carbon dioxide variations at Mauna Loa Observatory, Hawaii, Tellus, 28, 538–551, 1976.

Keeling, C. D., Bacastow, R. B., Carter, A. F., Piper, S. C., Whorf,

T. P., Heimann, M., Mook, W. G., and Roeloffzen, H.: A three-dimensional model of atmospheric CO_2transport based on observed winds. I: Analysis of observed data, American Geophysical Union, Washington D.C., 165–236, 1989.

Levine, M. D. and Aden, N. T.: Global carbon emissions in the coming decades: The Case of China, Ernest Orlando Lawrence Berkeley National Laboratory, 2008.

Marland, G., Boden, T. A., and Andres, R. J.: Global, regional, and national CO_2 emissions, Carbon Dioxide Inf. Anal. Cent., Oak Ridge Natl. Lab., U.S. Dep. of Energy, Oak Ridge, Tenn., 2007.

Murayama, S., Saigusa, N., Chan, D., Yamamoto, S., Kondo, H., and Eguchi, Y.: Temporal variations of atmospheric CO_2 concentration in a temperate deciduous forest in central Japan, Tellus B, 55, 232–243, 2003.

National Bureau of Statistics: China Statistical Yearbook 2008, China Stat. Press, Beijing, 2009.

National Development and Reform Commission (NDRC): Overview of the 11th Five Year Plan for National Economic and Social Development, Beijing, 2006.

Newell, R. E. and Evans, M. J.: Seasonal changes in pollutant transport to the north pacific: The relative importance of Asian and European sources, Geophys. Res. Lett., 27, 2509–2512, 2000.

Novelli, P. C. and Masarie, K. A.: Atmospheric Carbon Monoxide Dry Air Mole Fractions from the NOAA ESRL Carbon Cycle Cooperative Global Air Sampling Network, 1988–2009, Version: 2010-07-14, Path: ftp://ftp.cmdl.noaa.gov/ccg/co/flask/event/, 2010.

Piao, S. L., Fang, J. Y., Ciais, P., Peylin, P., Huang, Y., Sitch, S., and Wang, T.: The carbon balance of terrestrial ecosystems in China, Nature, 458, 1009–1082, 2009.

Potosnak, M. J., Wofsy, S. C., Denning, A. S., Conway, T. J., Munger, J. W., and Barnes, D. H.: Influence of biotic exchange and combustion sources on atmospheric CO_2 concentrations in New England from observations at a forest flux tower, J. Geophys. Res.-Atmos., 104, 9561–9569, 1999.

Streets, D. G., Bond, T. C., Carmichael, G. R., Fernandes, S. D., Fu, Q., He, D., Klimont, Z., Nelson, S. M., Tsai, N. Y., Wang, M. Q., Woo, J. H., and Yarber, K. F.: An inventory of gaseous and primary aerosol emissions in Asia in the year 2000, J. Geophys. Res.-Atmos., 108(D21), 8809, doi:10.1029/2002JD003093, 2003.

Streets, D. G., Zhang, Q., Wang, L., He, K., Hao, J., Wu, Y., Tang, Y., and Carmichael, G. R.: Revisiting China's co emissions after the transport and chemical evolution over the pacific (TRACE-P) mission: Synthesis of inventories, atmospheric modeling, and observations, J. Geophys. Res., 111, D14306, doi:10.1029/2006JD007118, 2006.

Suntharalingam, P., Jacob, D. J., Palmer, P. I., Logan, J. A., Yantosca, R. M., Xiao, Y. P., Evans, M. J., Streets, D. G., Vay, S. L., and Sachse, G. W.: Improved quantification of Chinese carbon fluxes using CO_2/CO correlations in Asian outflow, J. Geophys. Res.-Atmos., 109, D18S18, doi:10.1029/2003JD004362, 2004.

Tans, P. P., Fung, I. Y., and Takahashi, T.: Observational constraints on the global atmospheric CO2 budget, Science, 247(4949), 1431–1438, 1990.

Taguchi, S.: A three-dimensional model of atmospheric CO_2 transport based on analyzed winds: Model description and simulation results for TRANSCOM, J. Geophys. Res.-Atmos., 101, 15099–15109, 1996.

Thoning, K. W., Tans, P. P., and Komhyr, W. D.: Atmospheric carbon dioxide at Mauna Loa observatory 2. Analysis of the NOAA GMCC data, 1974–1985, J. Geophys. Res., 94, D6, 8549–8566, 1989.

Turnbull, J. C., Miller, J. B., Lehman, S. J., Tans, P. P., Sparks, R. J., and Southon, J.: Comparison of (CO_2)-C-14, CO, and SF_6 as tracers for recently added fossil fuel CO_2 in the atmosphere and implications for biological CO_2 exchange, Geophys. Res. Lett., 33, L01817, doi:10.1029/2005GL024213, 2006.

Wang, S. X., Zhao, M., Xing, J., Wu, Y., Zhou, Y., et al.: Quantifying the air pollutants emission reduction during the 2008 Olympic Games in Beijing, Environ. Sci. Technol. 44, 2490–2496, 2010b.

Wang, Y. X., Hao, J. M., McElroy, M. B., Munger, J. W., Hong, M., and Nielsen, C. P.: Year round measurements of O_3 and CO at a rural site near Beijing: seasonal variations and relationships, Tellus, 62B, 228–241, 2010.

Wang, Y., McElroy, M. B., Munger, J. W., Hao, J., Ma, H., Nielsen, C. P., and Chen, Y.: Variations of O_3 and CO in summertime at a rural site near Beijing, Atmos. Chem. Phys., 8, 6355–6363, doi:10.5194/acp-8-6355-2008, 2008.

Wang, Y., Hao, J., McElroy, M. B., Munger, J. W., Ma, H., Chen, D., and Nielsen, C. P.: Ozone air quality during the 2008 Beijing Olympics: effectiveness of emission restrictions, Atmos. Chem. Phys., 9, 5237–5251, doi:10.5194/acp-9-5237-2009, 2009.

Wofsy, S. C., Goulden, M. L., Munger, J. W., Fan, S. M., Bakwin, P. S., Daube, B. C., Bassow, S. L., and Bazzaz, F. A.: Net exchange of CO_2 in a midlatitude forest, Science, 260(5112), 1314–1317, 1993

Zhang, H. B., Yang, G. X., and Xin, X. P.: Studies on the changes in vegetation coverage of Xilinhaote grassland, Chinese Journal of Agricultural Resources and Regional Planning, 28, 42–46, 2007.

Zhang, X., Nakazawa, T., Ishizawa, M., Shujiaoki, Nakaoka, S., Sugawara, S., Maksyutov, S., Saeki, T., and Hayasaka, T.: Temporal variations of atmospheric carbon dioxide in the southernmost part of Japan, Tellus B, 59(4), 654–663, 2009.

Zhang, Q., Streets, D. G., Carmichael, G. R., He, K. B., Huo, H., Kannari, A., Klimont, Z., Park, I. S., Reddy, S., Fu, J. S., Chen, D., Duan, L., Lei, Y., Wang, L. T., and Yao, Z. L.: Asian emissions in 2006 for the NASA INTEX-B mission, Atmos. Chem. Phys., 9, 5131–5153, doi:10.5194/acp-9-5131-2009, 2009.

Zhou, L., White, J. W. C., Conway, T. J., Mukai, H., MacClune, K., Zhang, X., Wen, Y., and Li, J.: Long-term record of atmospheric CO_2 and stable isotopic ratios at Waliguan observatory: Seasonally averaged 1991–2002 source/sink signals, and a comparison of 1998-2002 record to the 11 selected sites in the northern hemisphere, Global Biogeochem. Cy., 20, GB2001, doi:10.1029/2004GB002431, 2006.

Zhou, L. X., Tang, J., Wen, Y. P., Li, J. L., Yan, P., and Zhang, X. C.: The impact of local winds and long-range transport on the continuous carbon dioxide record at mount Waliguan, China, Tellus B, 55, 145–158, 2003.

Zhou, L. X., Conway, T. J., White, J. W. C., Mukai, H., Zhang, X. C., Wen, Y. P., Li, J. L., and MacClune, K.: Long-term record of atmospheric CO_2 and stable isotopic ratios at Waliguan observatory: Background features and possible drivers, 1991–2002, Global Biogeochem. Cy., 19, GB3021, doi:10.1029/2004GB002430, 2005.